CSIRO PUBLISHING

Environ. Chem. **2016**, *13*, 902–912
http://dx.doi.org/10.1071/EN16046

Research Paper

Comparative evaluation of iron leach from different sources of fly ash under atmospherically relevant conditions

Jaya Borgatta,[A] *Amanda Paskavitz,*[A] *Deborah Kim*[A] *and Juan G. Navea*[A,B]

[A]Chemistry Department, Skidmore College, Saratoga Springs, NY 12866-1632, USA.
[B]Corresponding author. Email: jnavea@skidmore.edu

Environmental context. Iron, a limiting nutrient of plankton in the ocean, is deposited to the sea from atmospheric aerosols. In particular, atmospheric acidic conditions promote dissolution of iron from fly ash, a by-product of coal-fired power plants. Here, we report that the iron leached from fly ash depends on its source region, and that the type of combustion process may influence the iron species mobilized.

Abstract. Fly ash, an iron-containing by-product of coal-fired power plants, has been observed in atmospheric aerosol plumes. Under the acidic atmospheric conditions resulting from the uptake of atmospheric gases, iron leached from fly ash can impact global biogeochemical cycles. However, the fly ash source region, as well as its generating power plant, plays an important role in the amount, speciation and lability of iron. Yet no comparative studies have been made on iron leached from fly ash from different sources. This study reports the iron mobilisation by proton-promoted dissolution from well-characterised fly ash samples from three distinctive locations: the USA Midwest, north-east India and Europe. In addition, pH dependency was also investigated. Proton-promoted dissolution showed a variability between source regions with a relative iron leach in the order USA Midwestern > north-east Indian > European ash. In addition, the initial rate of iron leach suggests that source region is indeed a determining factor in the iron leaching capacity of fly ash, because dissolution from Midwestern fly ash is also faster than both European and Indian ash. Finally, the combustion process of fly ash proved to be significant for the iron speciation, given that well-combusted fly ash samples leached mostly Fe^{3+} rather than bioavailable Fe^{2+}. The role of fly ash should therefore be taken into account in order to better understand the effects of combustion particles in atmospheric iron deposition.

Additional keywords: aerosols, acidic processing, combustion particles, dissolution.

Received 29 February 2016, accepted 30 May 2016, published online 6 July 2016

Introduction

Over the last few decades, the global production of fly ash, a by-product of coal-fired power plants, has risen.[1] In the early 1990s, fly ash production was estimated at over 300 Tg per year worldwide.[2] Recent annual estimates indicate that the production of fly ash in the United States is ~66 Tg, 90 Tg in China and India each, and over 31 Tg in Europe.[3–6] Although efforts have been made to dispose of fly ash and prevent its emission into the atmosphere, field studies performed over the last decade have found fly ash particles in isolated regions, suggesting long-range atmospheric transport.[7–10] All fly ash particles found in the atmosphere are fine particulate matter (<2.5 μm) released either by direct emission or by fugitive emissions from the handling of fly ash.[10–13] Because of its size and morphology, fly ash tends to have long residence times, long-range transport and high atmospheric lifetimes.[7,8,10] Owing to their high iron oxide content, these combustion particles have been suggested as a source of atmospheric aqueous iron.[13,14] In fact, anthropogenic aerosols, including fly ash, have been shown to contribute ~50 % of the iron deposited near industrial regions and at least 5 % over open oceans.[15]

Iron leach from tropospheric aerosols during atmospheric acidic processing has been suggested as a source of bioavailable iron, Fe^{2+}, in open oceans.[16,17] As a limiting nutrient in isolated regions of the ocean, Fe^{2+} stimulates phytoplankton growth and promotes the sequestration of atmospheric CO_2.[18–21] Thus, the wet deposition of Fe^{2+} from fly ash may impact climate fluxes.[22,23] Recently, laboratory studies on fly ash standards have shown that combustion anthropogenic aerosols may have a similar stimulatory effect on phytoplankton growth.[13,15,24] Specifically, Chen et al. have shown that fly ash standards leach iron ions under atmospherically relevant conditions.[13,25] These studies observed the leach of both Fe^{2+} and Fe^{3+} from fly ash, indicating that fly ash may contribute a significant fraction of iron to the atmosphere.[13,24,25] However, the availability of iron from fly ash depends closely on its minerology and particle size.[26] Moreover, fly ash chemical composition and particle morphology vary with the source region and combustion process employed. The mineralogy and particle size of fly ash are determined by the chemical composition of the coal employed in the power plant, as well as the combustion process parameters in the boiler, such as air supply, heat of the combustion and duration of the combustion.[27] Therefore, coal-fired power plants using coal extracted from different sources may produce fly ash particles with distinctive physicochemical properties and varying environmental implications. Yet there

is no comparative study on the leach and rate of dissolution of iron from fly ash from different source regions.

Recent studies have shown that other tropospheric aerosols, such as mineral dust, are a natural source of iron in oceans.[24–26,28] These laboratory studies suggest that 24-h proton-promoted iron solubility from mineral dust ranges between 4 and 14 % of the initial total iron content in the mineral sample.[28] In contrast to combustion particles, which are generated through a highly oxidative process, speciation of trace metals in mineral dust can show a higher fraction of reduced species.[27] In fact, proton-promoted iron dissolution from mineral dust has shown a fairly important fraction of Fe^{2+}, ranging between 5 and 38 % of the total iron leached from mineral dust, depending on the source region.[28] This fairly large fraction of Fe^{2+} has the potential to impact on the bioavailable iron mobility in the environment. However, combustion particle speciation is thought to depend not only on the source region but also on the boiler combustion efficiency.[26,27] Thus, a comparative study on the effect of combustion particles such as fly ash from distinctive sources and power plants is important to establish its impact in the environmental availability of iron.

In the present work, we investigate the initial leach rate and yield of Fe^{2+} and Fe^{3+} from fly ash samples from three different source regions: the United States, India and Europe. All samples were captured in the flue-gas stack before atmospheric acidic processes take place. The significant difference in location ensures a different coal and thermal power-plant boiler, providing a comparative element to this study. This study investigates the leach of iron from fly ash at pH 1 and 2, acidic conditions that simulate the deliquescent layer of an aerosol particle on the uptake of acidic atmospheric gases.

Experimental

Source materials

Three fly ash (FA) samples were obtained from coal-fired power plants located in different regions: the United States of America (USFA) from the Midwest region, Indian fly ash (INFA) from north-eastern India, and European fly ash (EUFA) from a commercially available standard of fly ash (BCR®-176R) obtained from the European Commission. All reagents employed for sample characterisation and dissolution experiments were analytical grade. All reagents were used without further purification.

Morphology and spectroscopy of fly ash

The morphology and bulk composition of the FA samples were investigated using scanning electron microscopy (JEOL 6480 LV) coupled with energy-dispersive X-ray analysis (SEM-EDX; Bruker-AXS). In addition, surface areas for all dust samples were determined using an 11-point N_2-BET (Brunauer–Emmett–Teller) adsorption isotherm that was acquired with a Quantachrome Nova 1200 surface-area analyser. The samples were evacuated overnight before the surface area measurement.

Bulk elemental composition analysis of FA particles was measured using Bruker Tracer III-SD X-ray fluorescence spectroscopy (XRF). In addition, total iron content of all three FA samples was measured by atomic absorption spectroscopy (AAS) using a PerkinElmer AAnalyst 800 spectrometer. Approximately 0.1 g of fly ash samples was acid-digested in Teflon vessels using a mixture of 5 mL HNO_3 and 3 mL H_2O_2. The vessels were tightly sealed and microwaved in a microwave digestion system (Ethos model, Milestone) for a two-stage digestion method as described by Iwashita et al.[28]

Total attenuated reflectance Fourier-transform infrared spectra (ATR-FTIR) of all fly ash samples were recorded with a single-beam Perkin–Elmer FTIR spectrometer, equipped with a ZnSe ATR element and a deuterated, L-alanine-doped triglycine sulfate (DLaTGS/KBr) detector. All samples were deposited on the ATR crystal by pressing the dry powder onto the ZnSe crystal surface. Typically, 400 scans were acquired at an instrument resolution of 4 cm^{-1} over the full spectral range extending from 800 to 4000 cm^{-1}. Prior to FTIR analysis, all fly ash samples were vacuum-dried overnight at 373 K.

Iron leach experiments

Dissolution of iron species from fly ash was performed on fly ash suspensions of 1 g L^{-1}. Isothermal iron leach experiments were performed in a jacketed glass beaker at 298 K with constantly stirred solutions acidified with hydrochloric acid to a controlled pH set to 1.0 ± 0.1 or 2.0 ± 0.1. These conditions simulate cloud processing of tropospheric aerosol particles.[29] Note, Fe^{3+} shows low solubility above pH 3.6.[30] The solubility product of concentrations above 60 ppm, a concentration relevant for our iron leach experiments, Fe^{3+} begins to precipitate as $Fe(OH)_3$ above pH 2.4. In fact, increases in pH above this threshold of 2.4 have shown ferric iron precipitation in aqueous solutions with concentrations of Fe^{3+} of ~60 ppm.[31] Thus, an upper pH limit of 2.0 ± 0.1 allows the measurement of Fe^{3+} in solution without hydrolysis loss of iron.[25]

Even though the rate of ferrous iron oxidation is slow, its dependency on pH can lead to oxidation of Fe^{2+}, particularly as the pH increases.[32] Thus, in order to prevent oxidation of Fe^{2+} once leached from fly ash, all dissolution experiments were carried out under constant nitrogen purge to prevent oxidation by dissolved atmospheric oxygen.[31] This oxygen-free environment allowed a better quantification of both Fe^{3+} and Fe^{2+} leached from fly ash samples during the suspension experiments. In addition, to control the variations in ion strength in the suspension solution as the dissolution of fly ash particles took place, all acidic solutions were adjusted to an activity of 1 N NaCl.

Kinetic measurements started at time $t = 0$ min, defined as the moment of fly ash loading into the solution. After $t = 0$ min, aliquots of the suspension were taken periodically, filtered with a 0.2-μm filter, and colorimetrically analysed for dissolved iron content.[33] Dissolved iron speciation was quantified using 1,10-phenanthroline, which forms an orange complex with Fe^{2+} with an absorbance band at 510 nm. Total dissolved iron was quantified in the same samples by adding hydroxylamine to reduce all Fe^{3+} to Fe^{2+} before phenanthroline complexation. For the colorimetric calibration, primary standard ammonium iron(II) sulfate hexahydrate was used to prepare aqueous standard solutions of Fe^{2+} at a concentration range from 0.1 to 10 ppm. Hydroxyl ammonium sulfate was also added to each standard solution as a reducing agent, ensuring the presence of Fe^{2+} only. On addition of 1,10-phenanthroline solution, a 10-min passivation time was allowed before the absorbance measurement for every standard and sample. All colorimetric complexes absorbances were measured in a Lambda 35 Perkin–Elmer UV-vis spectrophotometer.

Results and discussions

Morphological study of fly ash samples

Particle size and morphology have been shown to have important implications in the leaching of iron from aerosol particles.

In general, as particles become smaller, a greater proportion of their surface is in physical contact with the acid media and, consequently, available for dissolution.[34] In addition, surface defects and porosity can increase acid media contact area, potentially increasing the initial rate and yield of particle dissolution. In particular, the predominantly spherical particles composing fly ash, which are the result of a controlled combustion process characteristic of high-efficiency power plants, offer a fairly large contact area between surface and proton. As the size of the particles increases, their exposed surface area decreases and their surface–proton contact area drops; nevertheless, as more defects are present in the particles, the surface–acid contact area increases.[34] Therefore, in order to better understand iron leach from the dissolution of the fly ash particles, specific surface area and particle size were investigated.

Specific surface areas, S_{BET}, of the three fly ash samples examined are 1.8 ± 0.1, 0.98 ± 0.03 and 2.8 ± 0.1 m^2 g^{-1} for USFA, INFA and EUFA respectively. Most particles examined in the fly ash samples were spherical in shape; however, EUFA showed a high proportion of irregular-shaped particles. The relatively high fraction of non-spherical particles found in EUFA suggests an incomplete combustion process, because a higher fraction of spherical particles is an indication of a thorough combustion process.[13] In general, particles are observed to aggregate, with clusters of smaller particles attached onto larger ones, as seen in the micrograph for the fly ash samples investigated in Fig. 1. Overall, the specific surface area indicates that EUFA will have a larger area exposed to the acidic media, whereas INFA will have a smaller area in contact with the aqueous phase.

Each micrograph shown in Fig. 1 has an elemental mapping that corresponds to the same micrograph, which shows that particles have a homogeneous distribution of minerals containing aluminium, silicon and iron in the spherical particles. In addition, the elemental composition of particles of different sizes is also homogeneous, with no significant difference in the elemental composition between particles of different sizes, consistent with observations made on standard fly ash samples.[12,13]

Fig. 2 shows the size distribution of fly ash particles examined. All size distributions consider only spherically shaped particles, even in EUFA, which has significant number of irregular-shaped particles. In general, spherical particles show a good fit to a log-normal size distribution,[35] as described by Eqn 1:

$$\left(\frac{dn}{d(d)}\right) = \left(\frac{dn}{d(d)}\right)_0 + \frac{A}{dw\sqrt{2\pi}} e^{\frac{-\left[\ln\frac{d}{\bar{d}}\right]^2}{2w^2}} \quad (1)$$

where n is the number of particles, $\left(\frac{dn}{d(d)}\right)$ is the normalised particle diameter, A and w are the amplitude and width of the normal distribution, d is the particle diameter and $\bar{d}$ is the arithmetic mean of the particle diameter. For each sample examined, $\bar{d}$ was determined from a sample of at least 350 particle counts, yielding values of (1.59 ± 0.05), (2.07 ± 0.04) and (4.6 ± 0.2) μm for USFA, INFA and EUFA respectively. The modal diameter, d_m, corresponds to the maxima in the log-normal fit shown in Fig. 2, and it represents the most probable particle diameter in each sample. The d_m was determined from the optimisation of the log-normal particle size distribution, the first-order derivative of Eqn 1:

$$\frac{d\left(\frac{dn}{d(d)}\right)}{dd} = 0 \Rightarrow d_m = \bar{d}e^{w^2} \quad (2)$$

As expected, the maxima in the log-normal modal suggest that the distribution diameters yield values below the arithmetic mean: 0.89 ± 0.08, 1.21 ± 0.06 and 2.2 ± 0.3 μm for USFA, INFA and EUFA respectively. The higher proportion of particles represented by the maxima in the plots in Fig. 2 is ~50 % smaller that the particle size median. Thus, fly ash samples examined have a size distribution and average size representative of those fly ash particles found in the atmosphere, with sizes <2.5 μm.[11,12]

The probability of smaller particles in the fly ash samples, as suggested by modal diameters, can have important implications in the iron leach on acidic processing. A greater abundance of smaller particles may lead to enhancements in particle dissolution and iron leach, because the available surface–acid interface that leads to the metal leach is inherently larger in smaller particles.[26,36,37] In addition, particle defects and porosity will tend to increase the surface available for reaction with H^+ ions during the particle acidic processing, which can play an important role in iron solubility.[34]

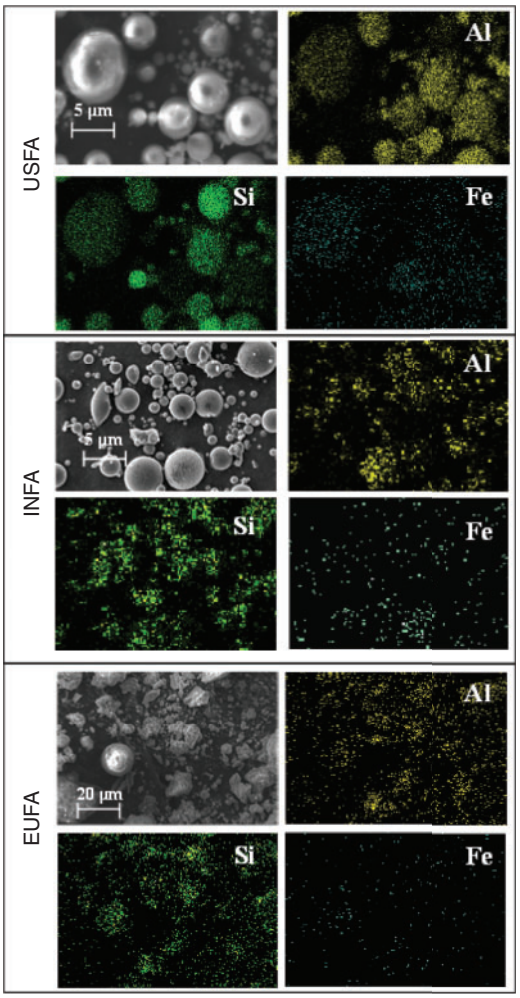

Fig. 1. Representative micrographs and corresponding Al, Si and Fe elemental maps obtained from scanning electron microscopy–energy-dispersive X-ray analysis (SEM-EDX) analysis of fly ash samples (USFA, United States fly ash; INFA, north-east Indian fly ash; EUFA, European fly ash).

An evaluation of the available surface with respect to the sphericity of the particles, ψ, allows a comparative assessment of the surface defects of the particles and the combustion process that produced the fly ash samples. The sphericity, as proposed by Wadell,[38] is a dimensionless parameter that was estimated as the ratio of the arithmetic mean diameter of the particles, $\bar{d}$, to the geometric diameter of a perfect sphere calculated from the specific surface areas determined through BET, d_{BET}:

$$\psi = \frac{\bar{d}}{d_{BET}} \Rightarrow \psi = \frac{\pi \bar{d}^2}{S_{BET}} \quad (3)$$

For the purpose of the present study, ψ values lower than 1 are a good indicator of a large number of surface defects and porosity rather than just particle shape. Indeed, given the defects observed through micrographs, all ψ values are significantly lower than 1. USFA and INFA were found to have sphericity values of $(2.1 \pm 0.1) \times 10^{-6}$ and $(3.7 \pm 0.1) \times 10^{-6}$, indicating that USFA has larger surface defects, allowing a larger physical contact between the particle surface and the acid media. However, the ψ ratio for EUFA was found to be $(4.9 \pm 0.3) \times 10^{-6}$. For USFA and INFA samples, where the particles are mostly spherical, the low ψ values are an indication of surface defects and porosity. Moreover, EUFA has a smaller specific surface area than suggested by the spherical particles owing to partially combusted particles. Table 1 summarises the morphological parameters in all fly ash samples.

Although the physical contact between particle surface and the acid media suggests a greater surface–proton interaction for USFA, where the largest deviation from a spherical surface is observed, the chemical composition of the particles indicates the effectiveness of the surface–proton interaction towards particle dissolution.

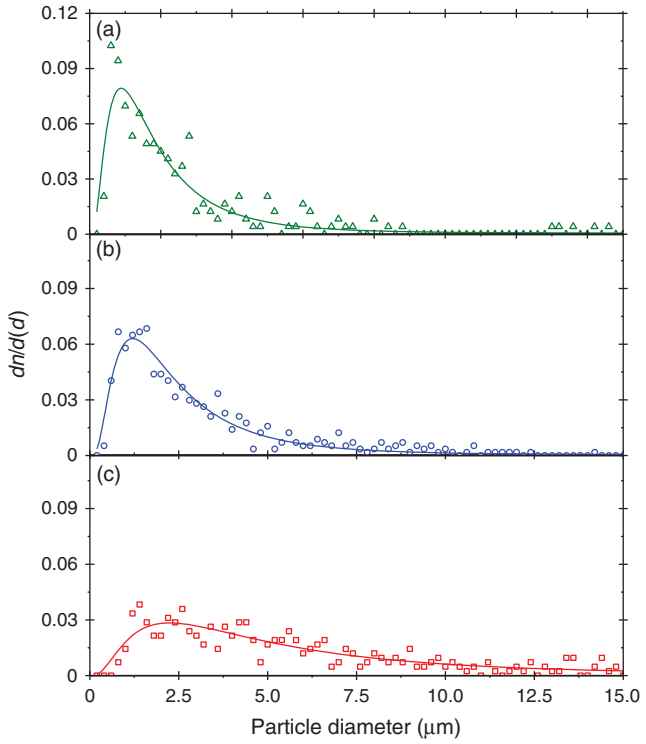

Fig. 2. Log-normal size distribution of (a) American Midwestern fly ash (USFA); (b) north-east Indian fly ash (INFA); and (c) European fly ash (EUFA). Histograms are the result of random micrograph selection and at least 350 particles measured.

Elemental composition

XRF shows a relative higher bulk content of iron than any other trace element. Table 2 summarises the bulk elemental composition of trace elements in all three fly ash samples, normalised without Al or Si. The difference in trace elemental composition in the bulk can be attributed to differences in coal mineralogy for the different regions.

In general, the relative content of iron, with respect to other trace elements, was found to be lower in European fly ash, whereas the largest was found in Indian fly ash. In fact, other than Al, Si and Fe, INFA has less than 5 % of all other trace elements. However, both USFA and EUFA showed a relatively higher content of Ca, with a higher content of Zn in EUFA.

When analysed using AAS, the content of total iron was found to be 38 ± 2, 25 ± 3 and 9.4 ± 0.8 mg g^{-1} for USFA, INFA, and EUFA respectively. The higher amount of iron in USFA indicates that INFA has a smaller proportion of trace elements relative to USFA. Thus, INFA has a relatively significant fraction of aluminosilicates in its bulk composition, where Al and Si are outside the XRF detection range and not shown in Table 2. Overall, atomic spectroscopy indicates that the largest amount of iron is found in United States fly ash, whereas European ash has the lowest content of iron. However, the

Table 2. X-ray fluorescence spectroscopy (XRF) elemental percentage of the major crustal elements in fly ash samples

The elemental analysis omits major components Al and Si. Error represents the standard deviation over triplicate measurements. USFA, United States fly ash; INFA, north-east Indian fly ash; EUFA, European fly ash

	%Fe	%Ca	%Zn	%Ti	%Sr
USFA	40 ± 1	35.8 ± 0.2	1.0 ± 0.1	3.6 ± 0.1	10.5 ± 0.4
INFA	74 ± 3	4.3 ± 0.1	1.0 ± 0.1	5.0 ± 0.1	2 ± 2
EUFA	11.6 ± 0.6	29 ± 1	28 ± 1	3.7 ± 0.2	1.7 ± 0.1

Table 1. Morphology summary of fly ash samples: United States fly ash (USFA), north-east Indian fly ash (INFA), and European fly ash (EUFA)

	Mean diameter, $\bar{d}$ (μm)	Most probable diameter, d_m (μm)	BET surface area, S_{BET} (m^2 g^{-1})	Sphericity, ψ ($\times 10^{-6}$)	Observation
USFA	1.59 ± 0.05	0.89 ± 0.08	1.8 ± 0.1	2.1 ± 0.1	Largest surface area due to smaller particle size
INFA	2.07 ± 0.04	1.21 ± 0.06	0.98 ± 0.03	3.7 ± 0.1	Smallest surface area due to larger particle size
EUFA	4.6 ± 0.2^{A}	2.2 ± 0.3^{A}	2.8 ± 0.1	4.9 ± 0.3	Smallest fraction of spherical particles due to incomplete combustion. Highest surface area due to surface defects

[A]Value obtained from spherical particles only.

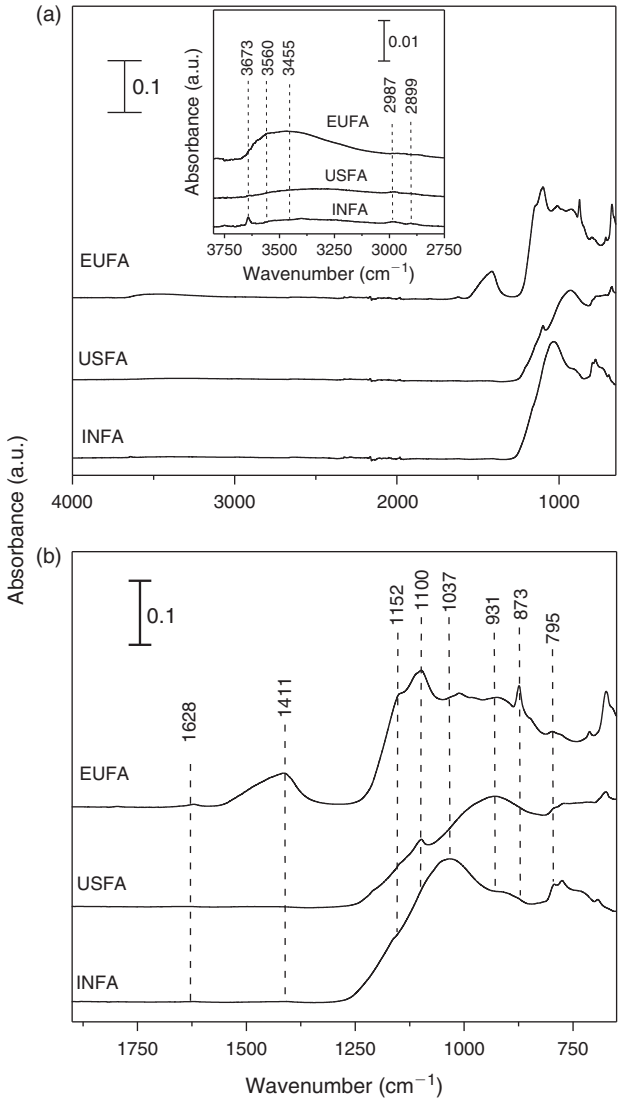

Fig. 3. (a) Attenuated total reflection Fourier-transform infrared (ATR-FTIR) spectra showing all three authentic fly ashes: United States fly ash (USFA); north-east Indian fly ash (INFA); and European fly ash (EUFA). The inset shows a magnified view of the spectral region from 2750 to 3800 cm^{-1}. (b) Spectral region from 650 to 1850 cm^{-1}.

incomplete combustion of EUFA suggests an iron speciation with a higher proportion of Fe^{2+} relative to that in USFA and INFA, because inefficient combustion will not completely oxidise all Fe^{2+} contained in coal samples.[15]

ATR-FTIR spectroscopy of fly ash samples

ATR-FTIR spectroscopy provides insight into the composition and chemical properties of the ash samples. The spectra of the dried fly ash samples are shown in Fig. 3.

Fig. 3a shows the entire region from 700 to 4000 cm^{-1}, with an insert showing an expansion of the region from 2750 to 3800 cm^{-1} whereas Fig. 3b shows a magnified view of the region from 700 to 1750 cm^{-1}. Based on previous literature assignments, the vibrational absorption bands are assigned to fundamental vibrational modes in Table 3.

The inset in Fig. 3a shows a band centred at ~3673 cm^{-1} for both Indian and European fly ash, assigned to the ν(OH) of structural hydroxyl groups. These spectral features suggest that both EUFA and INFA have the potential for formation of relatively more hydrogen bonds on surfaces than USFA. In addition, EUFA shows additional inner structural hydroxyl bands in the region of 3600 cm^{-1} not observed in either USFA or INFA. In particular, EUFA shows a broad band attributed to the hydrogen bonding stretching region at ~3455 cm^{-1} due to H-bonded hydroxyl groups. This observation indicates that the mineralogy of EUFA contains non-combusted particles with many interlayers capable of adsorbing water and interacting with H^+ ions in the acidic solutions.[39,40]

In Fig. 3b, European fly ash shows absorption bands in the 1400 cm^{-1} region, assigned to the bending mode of carbonates. In addition, EUFA shows a characteristic band at 1628 cm^{-1} due to the stretching vibration of –COO– of bicarbonates.[41] These carbonate and bicarbonate spectral features are absent in both United States and Indian fly ashes, indicating the fairly poor combustion of EUFA, as suggested by the higher presence of non-spherical particles seen in the micrographs shown in Fig. 1.

All fly ash samples show bands in the spectral region from 900 to 1700 cm^{-1}, assigned to vibrational absorptions bands due to lattice stretching motions of Si–O. Fig. 3b shows differences in frequency and peak intensities over this region for the three fly ash samples. In particular, both USFA and EUFA show ν(Si–O) centred at 931 to 1100 cm^{-1}, contrasting with the same bands displayed at ~1037 and 1152 cm^{-1} for INFA. This difference can be attributed to the lattice structures. In addition, bands near 780 cm^{-1} were assigned to deformation modes of Fe^{3+} and alkaline earth, δ(FeCa–OH).[42] The bands at ~875 cm^{-1} were also deformation modes of Fe^{3+} associated with aluminium, δ(FeAl–OH). All fly ash samples showed iron content associated with alkaline earth elements or aluminium. Finally, spectra for all three samples showed δ(AlAl–OH) at 930 cm^{-1}. Overall, the ATR-FTIR spectra showed that Al and Si were abundant in all three fly ash samples, with some Fe. Moreover, the ATR-FTIR bands indicate the presence of Fe in the samples, which is likely in the oxidation state Fe^{3+} because this oxidation state is consistent with the combustion process that generates fly ash.[40] Thus, iron leach from fly ash particles was expected to contain more Fe^{3+}. In addition, spectral features suggest that all fly ash samples have exposed edge sites with Al–OH and Si–OH bond terminals,[43] which is consistent with literature reports of silica and mullite ($3Al_2O_3{\cdot}2SiO_2$) content in fly ash.[44] The formation of mullite and silica in fly ash has been suggested to follow a two-step mechanism during the combustion process, where kaolinite ($Al_2O_3{\cdot}2SiO_2{\cdot}2H_2O$) forms metakalin ($Al_2O_3{\cdot}2SiO_2$), and further combustion leads to mullite:

$$Al_2O_3{\cdot}2SiO_2{\cdot}2H_2O(s) \rightarrow Al_2O_3{\cdot}2SiO_2(s) + 2H_2O(g) \quad (4)$$

$$3(Al_2O_3{\cdot}2SiO_2)(s) \rightarrow 3Al_2O_3{\cdot}2SiO_2(s) + 4SiO_2(s) \quad (5)$$

where the loss of the well-crystallised aluminosilicate clay minerals leading to mullite and silica has been suggested to decrease the stability of the mineral, which can lead to faster dissolution rates in an acidic media.[13] Overall, the differences between ATR-FTIR spectra are a reflection of the variations in mineralogy due to the difference in power-plant efficiency and their coal source. The exposed surface available for dissolution will interact with protons and the aqueous phase as a function of its chemical composition and affinity towards water and acidic media. A sample with higher affinity towards dissolution will lead to higher iron dissolution rates.[34]

Table 3. Vibration mode assignments

n.o., not observed. Vibrational frequencies are reported in cm^{-1}. USFA, United States fly ash; INFA, north-east Indian fly ash; EUFA, European fly ash

Vibration assignment and mode description	USFA	INFA	EUFA	Literature
δ(FeCa–OH)	795, 771	777	795	785[41]
δ(AlFe–OH)	–	–	873	873,[54] 885[55]
δ(AlAl–OH)	925	914	915	916,[55] 920[54]
ν(Si–O)	989	1006	–	992,[55] 995,[54]
ν(Si–O)	1001	1037	1012	1008,[54] 1060,[54] 1027[55]
ν(Si–O)	1100	1152	1100	1116,[55] 1102[55]
$\nu_3(CO_3^{2-})$	n.o.	n.o.	1411	1410[55]
$\nu_4(CO_3^{2-})$	n.o.	n.o.	1450	1430[54,55]
$\nu(HCO_3^-)$	n.o.	n.o.	1628	1630–1620[41]
ν(OH) structural hydroxyl	n.o.	3673	n.o.	3626,[54] 3642,[56] 3698[55]

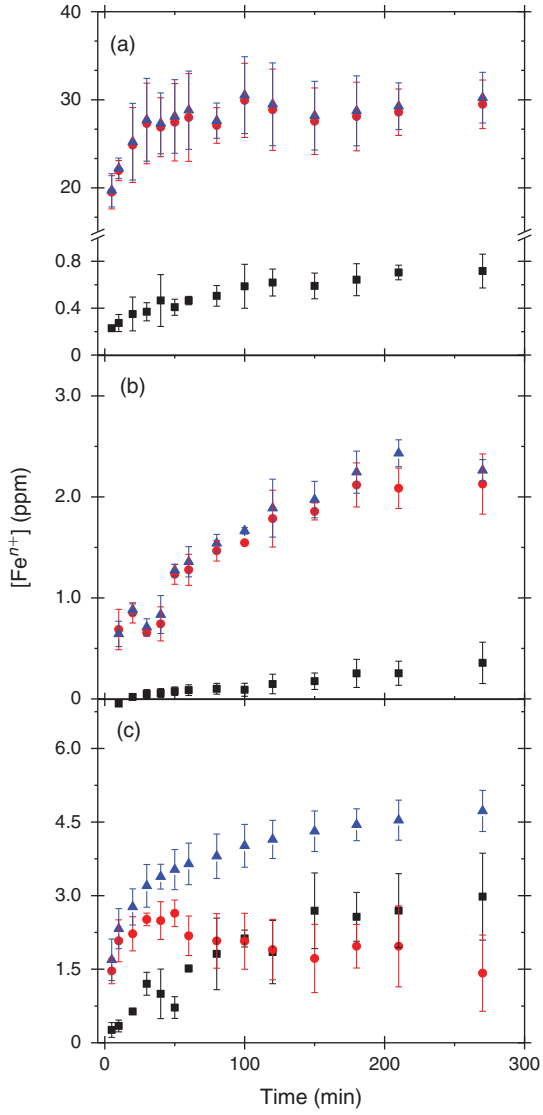

Fig. 4. Iron dissolution of 1.0 g L^{-1} of fly ash samples in acidified 1.0 M NaCl solutions at pH 1 as a function of time. ■ represents Fe^{2+}; ● represents Fe^{3+}; and ▲ represents total iron. Measured dissolved iron in (a) United States fly ash (USFA); (b) north-east Indian fly ash (INFA); and (c) European fly ash (EUFA) shows total dissolved iron, dissolved iron(II) and dissolved iron(III) for each sample. Error bars represent one standard deviation from triplicate experiments.

Iron leach experiments

Fly ash samples were allowed to dissolve in an acidic suspension, and periodically extracted aliquots were analysed colorimetrically for Fe^{2+} and Fe^{3+}. Fig. 4 shows the dissolution speciation of iron as a function of suspension time for the three different ashes examined at pH 1.0 ± 0.1. An increase in the concentration of both Fe^{2+} and Fe^{3+} was observed in all acid solutions. For the suspensions of USFA and INFA, the amount of Fe^{3+} in solution was higher than Fe^{2+} at any point of the dissolution experiment, as can be seen in Fig. 4a, b.

For comparison purposes, Table 4 summarises the iron speciation in the leach experiments at two different reference points: at 500 min of fly ash suspension in the acidic media, $[Fe^{n+}]_{500}$, and at 1440 min (1 day) of suspension, $[Fe^{n+}]_{1440}$. This finding supports the observation that Fe^{3+} is the predominant form of iron in fly ash, because the combustion process will favour the formation of Fe^{3+} oxide over Fe^{2+} species.[45] The relatively higher amount of Fe^{3+} oxides has been explained as the result of the complete combustion of pyrite ($Fe_{5/4}S$) and magnetite (Fe_3O_4, a mixture of Fe_2O_3 and FeO), common components of coal, through the following suggested two-step mechanism[46]:

$$\frac{4}{5}Fe_{5/4}S(s) + \frac{28}{15}O_2(g) \xrightarrow[\Delta]{} \frac{1}{3}Fe_3O_4(s) + \frac{4}{5}SO_2(g) \quad (6)$$

$$Fe_3O_4(s) + \frac{1}{4}O_2(g) \xrightarrow[\Delta]{} \frac{3}{2}Fe_2O_3(s) \quad (7)$$

Indeed, after 500 min of suspension, the concentration of Fe^{3+} in solution leached from USFA was nearly 31 times larger than that of Fe^{2+}, whereas INFA only showed detectable Fe^{3+} in solution. Leach of Fe^{2+} from the INFA suspension was only detectable after 700 min; before that time, the concentration of Fe^{2+} in solution was below 30 ppb, the limit of detection of the colorimetric method. In contrast, the suspension of EUFA in a pH 1 solution showed statistically similar concentrations of Fe^{3+} and Fe^{2+} between 80 min and 1440 min of reaction. As reported in Table 4, after 1440 min of EUFA suspension, the amount of Fe^{2+} leached into the solution became higher than the amount of Fe^{3+} found in solution. This supports the observation of an incomplete combustion of coal in the formation of the EUFA sample, as suggested by the micrographs and FTIR analysis (see above). The iron speciation in the solution phase in the EUFA suspension was the result of dissolution of iron-containing minerals in

Table 4. Concentration of iron species in solution leached from fly ash at 500 min of suspension, $[Fe^{n+}]_{500}$, and 1440 min of suspension, $[Fe^{n+}]_{1440}$
All concentrations are reported in parts per million. Errors represent standard deviations of data obtained from at least three experiments. USFA, United States fly ash; INFA, north-east Indian fly ash; EUFA, European fly ash

Fly ash	Iron concentration (ppm) at pH 1				Iron concentration (ppm) at pH 2			
	$[Fe^{2+}]_{500}$	$[Fe^{3+}]_{500}$	$[Fe^{2+}]_{1440}$	$[Fe^{3+}]_{1440}$	$[Fe^{2+}]_{500}$	$[Fe^{3+}]_{500}$	$[Fe^{2+}]_{1440}$	$[Fe^{3+}]_{1440}$
USFA	0.9 ± 0.3	27 ± 3	1.2 ± 0.2	31 ± 1	0.89 ± 0.05	21 ± 5	1.1 ± 0.1	25.2 ± 0.5
INFA	0.6 ± 0.3	2.7 ± 0.5	0.8 ± 0.4	6 ± 3	0.3 ± 0.2	1.46 ± 0.02	1.2 ± 0.4	2.6 ± 0.8
EUFA	3.2 ± 0.6	1.8 ± 0.8	4.4 ± 0.1	2.0 ± 0.6	1.2 ± 0.4	1.6 ± 0.1	2.2 ± 0.1	1.8 ± 0.8

Table 5. Initial rate of the fast (v_f) and slow (v_s) dissolution pathways of iron species leached from fly ash
n.o., not observed. Errors represent standard deviations of data obtained from at least three experiments. USFA, United States fly ash; INFA, north-east Indian fly ash; EUFA, European fly ash

pH	Sample	v_f ($\times 10^{15}$ molecules cm^{-3} s^{-1})			v_s ($\times 10^{13}$ molecules cm^{-3} s^{-1})		
		Fe^{2+}	Fe^{3+}	Total Fe	Fe^{2+}	Fe^{3+}	Total Fe
1	USFA	0.045 ± 0.004	3.8 ± 0.4	3.9 ± 0.4	0.062 ± 0.006	3.4 ± 0.8	3.5 ± 0.8
	INFA	n.o.	n.o.	n.o.	0.039 ± 0.002	0.21 ± 0.09	0.24 ± 0.09
	EUFA	0.05 ± 0.03	0.29 ± 0.05	0.33 ± 0.08	0.38 ± 0.05	0.43 ± 0.01	0.7 ± 0.1
2	USFA	n.o.	0.42 ± 0.05	0.42 ± 0.05	0.065 ± 0.006	4.3 ± 0.5	4.4 ± 0.6
	INFA	n.o.	n.o.	n.o.	0.021 ± 0.002	0.18 ± 0.02	0.20 ± 0.02
	EUFA	n.o.	n.o.	n.o.	0.18 ± 0.05	0.22 ± 0.02	0.33 ± 0.02

non-combusted coal particles, as well as the dissolution of both Fe^{3+} and Fe^{2+} in the partially combusted particles.

After a complete combustion process, the iron leach should yield Fe^{3+} only. However, the presence of both Fe^{3+} and Fe^{2+} in all fly ash suspension experiments was the product of iron oxides contained in magnetite, Fe_2O_3 and FeO, a common component in partially combusted coal as shown in Eqn 6, which can leach Fe^{2+}[45]:

$$\frac{1}{2}Fe_2O_3(s) + 3H^+(aq) \rightarrow Fe^{3+}(aq) + \frac{3}{2}H_2O(l) \quad (8)$$

$$FeO(s) + 2H^+(aq) \rightarrow Fe^{2+}(aq) + H_2O(l) \quad (9)$$

Fig. 4 suggests that iron dissolution from the fly ash samples examined was faster in USFA than in the other samples. Overall, the proton-promoted iron leach from fly ash suspensions exhibits two pathways: an initial, rapid iron leach on fly ash introduction into the pH 1 solution, followed by a slower leach of iron. The fast iron leach occurred on a time-scale faster than our experimental resolution and it was clearly observed in USFA and EUFA leach of total iron, whereas iron leaching from INFA did not show the faster iron dissolution pathway. The rapid dissolution suggested the presence of surface iron species interacting directly with protons through reactions similar to Eqns 8 and 9.[47] The fast pathway rate is extracted from the slope between $t = 0$ min and the first data point (5 min). However, the slower initial rate was taken from the slope of the linear segment from the first data point, $t = 5$ min, to the limit of linearity, which was determined from the deviation of the data point with respect to the linear extrapolation at a 95% level of confidence.[48] Based on our experimental resolution, the lower boundary of the initial rate of this rapid total iron ($Fe^{3+} + Fe^{2+}$) leach, v_f, was estimated to be $(3.9 \pm 0.4) \times 10^{15}$ molecules cm^{-3} s^{-1} and $(3.3 \pm 0.8) \times 10^{14}$ molecules cm^{-3} s^{-1} for USFA and EUFA at pH 1 respectively. In addition, iron leaching from fly ash slowly reached a plateau to a maximum iron leachate concentration in all cases. Considering the iron content in each fly ash sample examined, INFA yielded a considerably lower proportion of its iron content at a slower rate. These observations suggest that the mineralogy variations evidenced by the differences in the ATR-FTIR spectral features, a reflection of the coal source and combustion efficiency, play an important role in the leaching of iron.

The initial, fast leach of iron was followed by a slower leach attributed to the proton-promoted dissolution taking place as the result of H^+ ions interacting with particle surface functional groups, such as hydroxyl terminals and, in the case of the incomplete combustion particles found in EUFA, carbonates and hydroxyl groups.[49] As the proton complexes with the fly ash surface, it frees additional iron oxides or iron-containing incompletely combusted particles to continue the dissolution process.[13] The initial rate of the slower proton-promoted leach of iron, v_s, and the fast pathway, v_f, is summarised in Table 5.

The slow pathway of USFA is relatively faster than that in INFA, which mirrors the initial rate sequence observed for the fast pathway. It can be observed in Table 5 that the leaching of Fe^{2+} was slower than that of Fe^{3+}. The observed initial rate of the slow pathway, v_s, for each iron species has a different dependency on the pH:

$$v_s = \frac{d\left[Fe^{n+}_{(aq)}\right]}{dt} = k\left[H^+\right]^m \left[Fe^{n+}_{FA}\right] \quad (10)$$

where Fe^{n+}_{FA} is the iron available in fly ash present at the surface and in the bulk, $n = 2$ or 3 and m is the iron leach reaction order. Given the stoichiometric coefficients in Eqns 8 and 9, the initial rate of Fe^{3+} leach from the oxide particles primarily present in USFA and INFA was more susceptible to changes in pH than that of Fe^{2+} leach. Thus, because the pH was constant throughout the experiment, the initial rate of the second (slow) pathway, v_s was faster for the leach of Fe^{3+}, as indicated in the data

summarised in Table 5. In addition, ferrous iron is mostly found in the bulk of the particle rather than the surface. This suggests that, as the particle progressively dissolves and breaks down in the acidic solution, a higher fraction of Fe^{2+} species becomes available for acidic processing.[13] As a consequence, the dissolution initial rate of Fe^{2+} is dependent on the dissolution of the surface ferric iron.

The amount of Fe^{2+} leached from the EUFA suspension was the highest of the three samples examined. This observation is consistent the characterisation of EUFA particles, which showed an important fraction of non-combusted or partially combusted particles. Iron in non-combusted particles may have been present as part of the crystallised aluminosilicate composition, whereas partially combusted particles have been suggested to have an important magnetite (Fe_3O_4) fraction, as shown in Eqn 6.[46] In all these cases, the composition of the sample includes Fe^{2+}. Because the content of iron in EUFA was not necessarily in an oxide form, the initial rate was the result of a combination of Eqn 10 and the leaching of iron content in non-combusted particles. Contrary to the leaching of Fe^{3+} in the EUFA suspension, the leaching of Fe^{2+} did not undergo the fast pathway observed in USFA, suggesting that the dissolution of Fe^{2+} from EUFA samples was the result of bulk Fe^{2+} rather than surface iron. This observation suggests that Fe^{2+} was mostly contained in unburned minerals, because the combustion process did not consume the framework of the well-crystallised aluminosilicate to expose Fe^{2+}. Because the crystal aluminosilicate provides stability to the particles, no rapid dissolution of Fe^{2+} was possible. Overall, the initial slow rate of iron leach from EUFA suspension was slower than that from USFA, as summarised in Table 5.

Fig. 5 shows the dissolution speciation of iron for the three different fly ash samples examined at pH 2.0 ± 0.1. As observed in pH 1 suspensions, an increase in the concentration of both iron species was observed throughout the experiment. Overall, as expected from Eqn 8 and 9, the leach of iron slows down for all samples with the decrease in concentration of H^+ ions. In fact, the fast leach pathway observed in the pH 1 suspension of USFA and EUFA decreases substantially as the pH increases. In the case of USFA, the fast pathway was only observed in the leach of Fe^{3+}, whereas the fast pathway in EUFA was completely suppressed at pH 2. The fast initial rate of the total iron leach from USFA decreased from $(3.9 \pm 0.4) \times 10^{15}$ molecules cm^{-3} s^{-1} at pH 1 to $(4.2 \pm 0.5) \times 10^{14}$ molecules cm^{-3} s^{-1} at pH 2, a drop of ~90 %. Table 5 summarises the initial rate for both the slower proton-promoted leach of iron, v_s, and the fast pathway, v_f.

In addition, for pH 2 solutions the slow pathway rate showed a similar trend to that observed at pH 1, with USFA having the fastest dissolution rate and the slowest being in INFA. Table 5 summarises the initial rates for both pH 1 and pH 2. It can be seen that the values of v_s at pH 2 show no statistically significant change for the leach of total iron, Fe^{2+} and Fe^{3+} from USFA. However, v_s for the leach of total iron at pH 2 significantly dropped for the other samples studied, with a decline from pH 1 of 83 and 47 % for INFA and EUFA respectively. In all cases, the concentration of iron slowly reached a plateau to equilibrium concentrations.

In order to make a direct comparison of the iron leached from each fly ash sample, the concentration of total iron remaining in fly ash at a given suspension time t was calculated from the normalised concentration of total iron leached and the iron content in the fly ash loading, as determined by AAS analysis and the experimental suspended fly ash loading of 1 g L^{-1}:

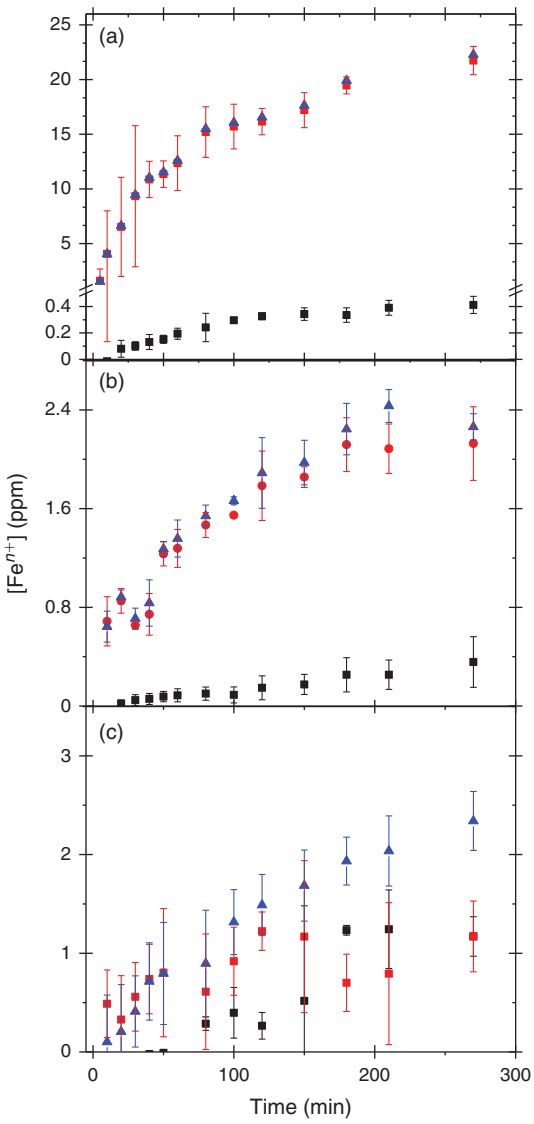

Fig. 5. Iron dissolution of 1.0 g L^{-1} of fly ash samples in acidified 1.0 M NaCl solutions at pH 2 as a function of time. ■ represents Fe^{2+}; ● represents Fe^{2+}; and ▲ represents total iron. Measured dissolved iron in (a) United States fly ash (USFA); (b) north-east Indian fly ash (INFA); and (c) European fly ash (EUFA) shows total dissolved iron, dissolved iron(II) and dissolved iron(III) for each sample. Error bars represent one standard deviation from triplicate experiments. See Fig. S1 in the Supplementary material for a results pertaining to data at pHs 1 and pH 2.

$$\text{Fraction of iron remaining in fly ash samples} = 1 - \frac{\left([Fe^{2+}]_t + [Fe^{3+}]_t\right)}{\left([Fe^{2+}]_{FA} + [Fe^{3+}]_{FA}\right)} \quad (11)$$

where $[Fe^{2+}]_{FA}$ and $[Fe^{3+}]_{FA}$ represent the concentration of iron (II) and iron(III) available in fly ash, and $[Fe^{2+}]_t$ and $[Fe^{3+}]_t$ represent the concentration of total iron(II) and iron(III) leached at a time t, respectively. Fig. 6 shows the time progression of the fraction of total iron remaining in the fly ash samples. Using Eqn 11, the fraction of total iron leached from USFA was estimated ~80 % beyond 500 min of suspension for both pH 1 and 2. Conversely, total iron dissolution from INFA was ~10 % for both pH 1 and 2. Finally, EUFA in pH 1 solutions reached a maximum fraction of iron leached at ~150 min of suspension, with a higher fraction of iron leached at pH 1.

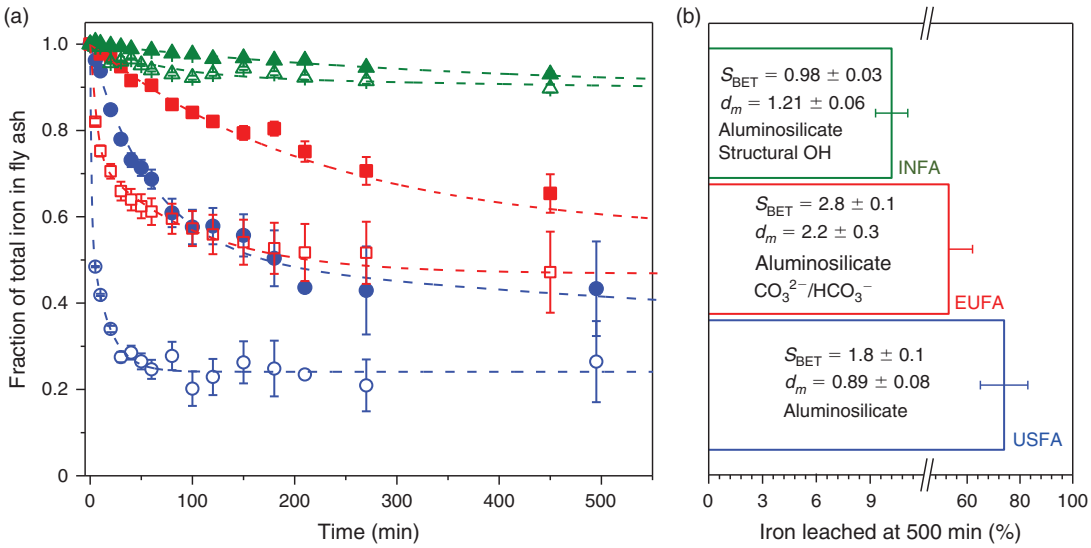

Fig. 6. (a) fraction of total iron in fly ash samples. Clear symbols represent the fraction of iron leached from fly ash suspensions in pH 1 solutions; full symbols represent the fraction of iron leached from fly ash suspensions in pH 2 solutions. Blue circles correspond to iron leached from United States fly ash (USFA); red squares correspond to iron leached from European fly ash (EUFA); and green triangles represent iron leached from north-east Indian fly ash (INFA). (b) Dissolution yield after 500 min of suspension in a pH 1 solution. d_m, is the modal diameter in μm and S_{BET} is the Brunauer–Emmett–Teller surface area of the sample in $m^2\ g^{-1}$.

Previous dissolution experiments at pH 1 that used fly ash standard materials with higher Fe^{2+} content than the samples used in the present study showed a total iron leaching of ~50 %.[13,25] Although this observation is consistent with the total iron leaching from EUFA, the sample with the largest leaching of ferrous ions, our results suggest that a combination of particle size and mineralogy, as well as the coal-combustion efficiency, plays an important role not only in the solubility of total iron but also in the iron speciation in the solution phase. In fact, Fig. 6b indicates that the dissolution yield does not correlate with a single property, suggesting that it is a combined effect of the mineralogy, surface area and morphology of the fly ash sample. Significantly, USFA, the fly ash sample with the largest relative iron content reported in the current work, shows the highest iron solubility at the fastest rates. In fact, the fast pathway at pH 1 for USFA accounted for over 50 % of the total iron leached. However, the fast pathway at pH 1 for EUFA accounted for ~18 % of total iron leached into solution. In addition, as observed in Figs 4 and 5, only a short fast pathway was observed at pH 2 in USFA, which accounted for only 2 % of the total iron leached. With the exception of EUFA samples, most of the total iron reported in Fig. 6 corresponded to Fe^{3+}. Finally, Fig. 6 shows that pH 1 total iron dissolution was consistently faster than at pH 2, because the fraction of total iron in fly ash reached a plateau earlier at the lower pH. This observation supports the rate dependency on the concentration of H^+, as expressed in Eqn 10. This result suggests that variability between fly ash source regions has distinctive atmospheric effects.

Conclusions

Recent field observations suggest that fly ash particles can be considered a source of atmospheric iron.[1,7,8,50] However, most laboratory studies available use fly ash standards, with no distinction between source regions of combustion process.[13,25] The comparative study we present here shows that the atmospheric acidic processing of three different fly ash samples from three different sources, the United States, India and Europe, yields significant variations in iron mobilisation. The proton-promoted dissolution of iron shows the relative percentage of iron leached from each sample is in the order USFA > EUFA > INFA. Compared with mineral dust dissolution, combustion aerosol samples may play a more important role in mobilising Fe^{3+} than Fe^{2+}.[26,51] Our study suggests that particles that are only partially combusted or not-well-combusted particles will leach bioavailable Fe^{2+} in the deliquescent layer of an aerosol particle on the uptake of acidic atmospheric gases. Thus, the combustion efficiency of coal-fired power plants plays a significant role in the speciation of iron mobilised by atmospheric acidic processing.

Our results also indicate that the impact of pH on the rate of iron dissolution varies significantly with the source region. In particular, USFA shows a two-step pathway of iron leaching: the initial rate of iron leached from USFA shows a pH effect only for an initial fast dissolution pathway; there is no statistically significant influence of pH for the slower pathway. Conversely, samples from India and Europe show mostly a single slow pathway, with a rate that drops when the solution acidity decreases from pH 1 to 2. This difference could be due to a higher proportion of surface and labile iron in USFA compared with that in INFA and EUFA. Nevertheless, changes in the pH continue to show the same proportion of iron speciation, showing a significantly higher proportion of acid-mobilised Fe^{3+} with respect of Fe^{2+}. In fact, the acidic processing of the fully combusted samples (USFA and INFA) examined in our work shows that for USFA, 93 % of the iron leached is Fe^{3+}, whereas for INFA, 88 % of the total iron leached is Fe^{3+}. On the basis of these results, it can be proposed that coal that is only partially combusted could be a significant source of bioavailable iron in the atmosphere. In order to better understand the biogeochemical cycle of atmospheric iron, additional reduction mechanisms of iron should be considered.[52,53]

Supplementary material

Iron dissolution data of the fly ash samples at pHs 1 and 2 are available from the journal online (see http://www.publish.csiro.au/?act=view_file&file_id=EN16046_AC.pdf).

Acknowledgements

Financial support from Skidmore College is gratefully acknowledged. The authors also acknowledge Matthew Lueckheide's assistance in the bulk iron analysis of fly ash samples using AAS.

References

[1] K. Ojha, N. C. Pradhan, A. N. Samanta, Zeolite from fly ash: synthesis and characterization. *Bull. Mater. Sci.* **2004**, *27*, 555. doi:10.1007/BF02707285

[2] O. E. Manz, Worldwide production of coal ash and utilization in concrete and other products. *Fuel* **1997**, *76*, 691. doi:10.1016/S0016-2361(96)00215-3

[3] *2013 Coal Combustion Product (CCP) Production & Use Survey Report* **2014** (American Coal Ash Association: Aurora, CO).

[4] E. Haque, Indian fly-ash: production and consumption scenario. *International Journal of Waste Resources* **2013**, *3*, 22. doi:10.12777/IJWR.3.1.2013.22-25

[5] H. J. Feuerborn, in *Coal Combustion Products in Europe – An Update on Production and Utilisation Standardization and Regulation*, *World of Coal Conference*, *Denver*, *CO, 9–12 May* **2011**.

[6] X. P. Cai, S. Q. Zhang, J. G. Li, in *Proceedings of the 2015 International Conference on Water Resources and Environment* **2015**, pp. 35–37 (CRC Press: Beijing).

[7] V. Ramanathan, P. J. Crutzen, J. T. Kiehl, D. Rosenfeld, Aersols, climate and the hydrological cycle. *Science* **2001**, *294*, 2119. doi:10.1126/SCIENCE.1064034

[8] J. Inoue, A. Momose, T. Okudaria, A. Murakami-Kitase, H. Yamazaki, S. Yoshikawa, Chemical characteristics of north-east Asian fly ash particles: implications for their long-range transportation. *Atmos. Environ.* **2014**, *95*, 375. doi:10.1016/J.ATMOSENV.2014.06.048

[9] P. Nowinski, V. F. Hodge, S. Gerstenberger, Application of field portable X-ray fluorescence to the analysis of desert varnish samples in areas affected by coal-fired power plants. *Environ. Chem.* **2012**, *9*, 379. doi:10.1071/EN11139

[10] M. O. Andreae, P. J. Crutzen, Atmospheric aerosols: biogeochemical sources and role in atmospheric chemistry. *Science* **1997**, *276*, 1052. doi:10.1126/SCIENCE.276.5315.1052

[11] W. Li, L. Shao, Transmission electron microscopy study of aerosol particles from the brown hazes in northern China. *Journal of Geophysical Research: Atmospheres* **2009**, *114(D9)*, D09302. doi:10.1029/2008JD011285

[12] S. F. Mueller, J. W. Mallard, Q. Mao, S. L. Shaw, Fugitive particulate emissions from a dry coal fly ash disposal. *J. Air Waste Manag. Assoc.* **2013**, *63*, 806. doi:10.1080/10962247.2013.795201

[13] H. Chen, A. Laskin, J. Baltrusaitis, C. A. Gorski, M. M. Scherer, V. H. Grassian, Coal fly ash as a source of iron in atmospheric dust. *Environ. Sci. Technol.* **2012**, *46*, 2112. doi:10.1021/ES204102F

[14] B. G. Kutchko, A. G. Kim, Fly ash characterization by SEM-EDS. *Fuel* **2006**, *85*, 2537. doi:10.1016/J.FUEL.2006.05.016

[15] C. Luo, N. Mahowald, T. Bond, P. Y. Chuan, J. Schauer, Combustion iron distribution and deposition. *Global Biogeochem. Cycles* **2008**, *22*, GB1012. doi:10.1029/2007GB002964

[16] R. A. Duce, N. W. Tindale, Atmospheric transport of iron and its deposition in the ocean. *Limnology and Oceanography* **1991**, *36*, 1715. doi:10.4319/LO.1991.36.8.1715

[17] S. Fan, W. J. Moxim, H. Levy, Aeolian input of bioavailable iron to the ocean. *Geophys. Res. Lett.* **2006**, *33*, L07602.

[18] I. Y. Fung, S. K. Meyn, I. Tegen, S. C. Doney, J. G. John, J. K. B. Bishop, Iron supply and demands in the upper ocean. *Global Biogeochem. Cycles* **2000**, *14*, 281. doi:10.1029/1999GB900059

[19] J. H. Martin, S. E. Fitzwater, Iron deficiency limits phytoplankton growth in the north-east Pacific Subarctic. *Nature* **1988**, *331*, 341. doi:10.1038/331341A0

[20] S. Bonnet, C. Guieu, Dissolution of atmospheric iron in seawater. *Geophys. Res. Lett.* **2004**, *31*, L03303.

[21] P. W. Boyd, A. J. Watson, C. S. Law, E. R. Abraham, T. Trull, R. Murdoch, D. C. E. Bakker, A. R. Bowie, K. O. Buesseler, H. Chang, M. Charette, P. Croot, K. Downing, R. Frew, M. Gall, M. Hadfield, J. Hall, M. Harvey, G. Jameson, J. LaRoche, M. Liddicoat, R. Ling, M. T. Maldonado, M. R. McKay, S. Nodder, S. Pickmere, R. Pridmore, S. Rintoul, K. Safi, P. Sutton, R. Strzepek, K. Tanneberger, S. Turner, A. Waite, J. Zeldis, A mesoscale phytoplankton bloom in the polar Southern Ocean stimulated by iron fertilization. *Nature* **2000**, *407*, 695. doi:10.1038/35037500

[22] U. Riebesell, D. A. Wolf-Gladrow, V. Smetacek, Carbon dioxide limitation of marine phytoplankton growth rates. *Nature* **1993**, *361*, 249. doi:10.1038/361249A0

[23] R. Lal, Carbon sequestration. *Phil. Trans. R. Soc. B* **2008**, *363*, 815. doi:10.1098/RSTB.2007.2185

[24] K. V. Desboeufs, A. Sofitkitis, R. Losno, L. Colin, P. Ausset, Dissolution and solubility of trace metals from natural and anthropogenic aerosol particulate metal. *Chemosphere* **2005**, *58*, 195. doi:10.1016/J.CHEMOSPHERE.2004.02.025

[25] H. Chen, V. H. Grassian, Iron dissolution of dust source materials during simulated acidic processing: the effect of sulfuric, acetic, and oxalic acids. *Environ. Sci. Technol.* **2013**, *47*, 10312.

[26] G. Rubasinghege, L. W. Robert, S. M. Michelle, V. H. Grassian, Simulated atmospheric processing of iron oxyhydroxide minerals at low pH: roles of particle size and acid anion in iron dissolution. *Proc. Natl. Acad. Sci. USA* **2010**, *107*, 6628. doi:10.1073/PNAS.0910809107

[27] L. Morawska, J. Zhang, Combustion sources of particles. 1. Health relevance and source signatures. *Chemosphere* **2002**, *49*, 1045. doi:10.1016/S0045-6535(02)00241-2

[28] D. Cwiertny, J. Baltrusaitis, G. Hunter, A. Laskin, M. M. Scherer, V. H. Grassian, Characterization and acid-mobilization study of iron-containing mineral dust source materials. *J. Geophys. Res.* **2008**, *113*, D05202. doi:10.1029/2007JD009332

[29] A. Iwashita, T. Nakajima, H. Takanashi, A. Ohki, Y. Fujita, T. Yamashita, Determination of trace elements in coal and coal fly ash by joint-use of ICP-AES and atomic absorption spectrometry. *Talanta* **2007**, *71*, 251. doi:10.1016/J.TALANTA.2006.03.053

[30] W. C. Keene, R. Sander, A. A. P. Pszenny, R. Vogt, P. J. Crutzen, J. N. Galloway, Aerosol pH in the marine boundary layer: a review and model evaluation. *J. Aerosol Sci.* **1998**, *29*, 339. doi:10.1016/S0021-8502(97)10011-8

[31] J. H. Seinfeld, S. N. Pandis, *Atmospheric Chemistry and Physics: From Air Pollution to Climate Change* **2006** (Wiley: Hoboken, NJ).

[32] D. C. Harris, *Exploring Chemical Analysis, 2nd edn* **1997** (WH Freeman and Company: New York, NY).

[33] W. Stumm, G. F. Lee, Oxygenation of ferrous iron. *Ind. Eng. Chem.* **1961**, *53*, 143. doi:10.1021/IE50614A030

[34] W. B. Fortune, M. G. Mellon, Determination of iron with *o*-phenanthroline: a spectrophotometric study. *Ind. Eng. Chem.* **1938**, *10*, 60.

[35] A. R. Baker, T. D. Jickells, Mineral particle size as a control on aerosol iron solubility. *Geophys. Res. Lett.* **2006**, *33*, L17608. doi:10.1029/2006GL026557

[36] J. Heintzenberg, Properties of the log-normal particle size distribution. *Aerosol Sci. Technol.* **1994**, *21*, 46. doi:10.1080/02786829408959695

[37] O. Laskina, H. S. Morris, J. R. Grandquist, Z. Qin, E. A. Stone, A. V. Tivanski, V. H. Grassian, Size matters in the water uptake and hygroscopic growth of atmospherically relevant multicomponent aerosol particles. *J. Phys. Chem. A* **2015**, *119*, 4489. doi:10.1021/JP510268P

[38] J. W. Mauchly, Significance test for sphericity of a normal *n*-variate distribution. *Ann. Math. Stat.* **1940**, *11*, 204. doi:10.1214/AOMS/1177731915

[39] J. D. Schuttlefield, D. Cox, V. H. Grassian, An investigation of water uptake on clay minerals using ATR-FTIR spectroscopy coupled with quartz crystal microbalance measurements. *J. Geophys. Res., D, Atmospheres* **2007**, *112*, D21303. doi:10.1029/2007JD008973

[40] J. Baltrusaitis, C. Usher, V. H. Grassian, Reactions of sulfur dioxide on calcium carbonate single-crystal and particle surfaces at the adsorbed water–carbonate interface. *Phys. Chem. Chem. Phys.* **2007**, *9*, 3011. doi:10.1039/B617697F

[41] L. Ferretto, A. Glisenti, Study of the surface acidity of an hematite powder. *J. Mol. Catal. Chem.* **2002**, *187*, 119. doi:10.1016/S1381-1169(02)00126-7

[42] H. D. Lutz, H. Möller, M. Schmidt, Lattice vibration spectra. Part LXXXII. Brucite-type hydroxides $M(OH)_2$ (M = Ca, Mn, Co, Fe, Cd) – IR and Raman spectra, neutron diffraction of $Fe(OH)_2$. *J. Mol. Struct.* **1994**, *328*, 121. doi:10.1016/0022-2860(94)08355-X

[43] K. L. Konan, C. Peyratout, J.-P. Bonnet, A. Smith, A. Jacquet, P. Magnoux, P. Ayrault, Surface properties of kaolin and illite suspensions in concentrated calcium hydroxide medium. *J. Colloid Interface Sci.* **2007**, *307*, 101. doi:10.1016/J.JCIS.2006.10.085

[44] S. C. White, E. D. Case, Characterization of fly ash from coal-fired power plants. *J. Mater. Sci.* **1990**, *25*, 5215. doi:10.1007/BF00580153

[45] J. Tomeczek, H. Palugniok, Kinetics of mineral matter transformation during coal combustion. *Fuel* **2002**, *81*, 1251. doi:10.1016/S0016-2361(02)00027-3

[46] S. Srinivasachar, J. J. Helble, A. A. Boni, Mineral behaviour during coal combustion 1. Pyrite transformations. *Pror. Energy Combust. Sci.* **1990**, *16*, 281. doi:10.1016/0360-1285(90)90037-4

[47] B. Zinder, G. Furrer, S. Werner, The coordination chemistry of weathering: II. Dissolution of Fe^{III} oxides. *Geochim. Cosmochim. Acta* **1986**, *50*, 1861. doi:10.1016/0016-7037(86)90244-9

[48] D. M. B. Lesko, E. M. Coddens, H. D. Swomley, R. M. Welch, J. Borgatta, J. G. Navea, Photochemistry of nitrate chemisorbed on various metal oxide surfaces. *Phys. Chem. Chem. Phys.* **2015**, *17*, 20775. doi:10.1039/C5CP02903A

[49] C. K. Remucal, D. L. Sedlak, The role of iron coordination in the production of reactive oxidants from ferrous iron oxidation by oxygen and hydrogen peroxide, in *Aquatic Redox Chemistry* (Ed. Paul G. Tratnyek, Timothy J. Grundl, Stefan B. Haderlein) **2011**, Vol. 1071, p. 177 (American Chemical Society: Washington, DC).

[50] B. Srinivas, M. M. Sarin, A. Kumar, Impact of anthropogenic sources on aerosol iron solubility over the Bay of Bengal and the Arabian Sea. *Biogeochemistry* **2012**, *110*, 257. doi:10.1007/S10533-011-9680-1

[51] C. R. Usher, A. E. Michel, V. H. Grassian, Reactions on mineral dust. *Chem. Rev.* **2003**, *103*, 4883. doi:10.1021/CR020657Y

[52] J. Borgatta, G. Navea, Fate of aqueous iron leached from tropospheric aerosols during atmospheric acidic processing: study of the effects of humic-like substances. *WIT Transactions of Ecology and the Environment* **2015**, *198*, 155. doi:10.2495/AIR150131

[53] H. A. Al-Abadleh, Review of the bulk and surface chemistry of iron in atmospherically relevant systems containing humic-like substances. *RSC Adv.* **2015**, *5*, 45785. doi:10.1039/C5RA03132J

[54] J. G. Navea, H. Chen, M. Huang, G. R. Carmichel, V. H. Grassian, A comparative evaluation of water uptake on several mineral dust sources. *Environ. Chem.* **2010**, *7*, 162. doi:10.1071/EN09122

[55] J. Madejová, P. Komadel, Baseline studies of the clay minerals society source clays: infrared methods. *Clays Clay Miner.* **2001**, *49*, 410. doi:10.1346/CCMN.2001.0490508

[56] H. Namduri, S. Nasrazadi, Quantitative analysis of iron oxides using Fourier-transform infrared. *Corros. Sci.* **2008**, *50*, 2493. doi:10.1016/J.CORSCI.2008.06.034